

Article

Atomic Scale Simulation on the Anti-Pressure and Friction Reduction Mechanisms of MoS₂ Monolayer

Yang Liu, Yuhong Liu *, Tianbao Ma and Jianbin Luo *

State Key Laboratory of Tribology, Tsinghua University, Beijing 100084, China; yang-liu@outlook.com (Y.L.); mtb@tsinghua.edu.cn (T.M.)

* Correspondence: liuyuhong@tsinghua.edu.cn (Y.L.); luojb@tsinghua.edu.cn (J.L.); Tel.: +86-10-6278-8387 (Y.L.); +86-10-6278-1385 (J.L.)

Received: 7 April 2018; Accepted: 26 April 2018; Published: 27 April 2018



Abstract: MoS₂ nanosheets can be used as solid lubricants or additives of lubricating oils to reduce friction and resist wear. However, the atomic scale mechanism still needs to be illustrated. Herein, molecular simulations on the indentation and scratching process of MoS₂ monolayer supported by Pt(111) surface were conducted to study the anti-pressure and friction reduction mechanisms of the MoS₂ monolayer. Three deformation stages of Pt-supported MoS₂ monolayer were found during the indentation process: elastic deformation, plastic deformation and finally, complete rupture. The MoS₂ monolayer showed an excellent friction reduction effect at the first two stages, as a result of enhanced load bearing capacity and reduced deformation degree of the substrate. Unlike graphene, rupture of the Pt-supported MoS₂ monolayer was related primarily to out-of-plane compression of the monolayer. These results provide a new insight into the relationship between the mechanical properties and lubrication properties of 2D materials.

Keywords: MoS₂ monolayer; indentation; rupture; scratch; friction; molecular dynamics

1. Introduction

2D materials, such as graphene, few-layer MoS₂ and black phosphorus, have shown great potential in many areas due to their special physical properties [1–5]. Their excellent mechanical performance [6,7] and high thermal conductivity [8], together with their flatness and thickness at the atomic scale [9], make some 2D materials ideal lubricants for certain areas [10], for example in micro- or nanoelectro-mechanical systems [11,12] and high density magnetic storage devices [13], where the lubricating space is limited and lubricating condition is severe [14], lubrication coatings of 2D materials are considered to be a good choice [15].

When used as lubricant additives or solid lubricants, graphene and few-layer MoS₂ can improve the extreme pressure (highest load without seizure of the friction pairs) and reduce the friction of rubbing surfaces [16,17]. These excellent lubricating properties, including the anti-pressure effect and friction reduction effect, are usually attributed to the better mechanical properties of 2D materials than metal friction pairs [18]. For instance, graphene has a Young's modulus of about 1000 GPa and a breaking strength of about 130 GPa, while the Young's modulus of stainless steel is only 205 GPa, with a breaking strength of 0.9 GPa [19]. Due to the high elastic modulus and breaking strength, graphene can share extra load and reduce friction before its rupture [20]. However, while the mechanical properties of the MoS₂ monolayer are not as excellent as those of graphene, with a Young's modulus of about 270 GPa and a breaking strength of about 30 GPa [19], the lubrication properties of few-layer MoS₂ seem to be better. Macroscopic lubrication experiments have shown that MoS₂ nanosheets can be more stable and effective than graphene when used as lubricant additives, with a lower friction coefficient [21] and higher extreme pressure [22]. The inconsistency of lubrication properties and

mechanical properties requires detailed research on the atomic mechanism of the anti-pressure and friction reduction effect of MoS₂ monolayer.

In this paper, in order to find out the anti-pressure mechanism of MoS₂ monolayer, indentation process of MoS₂ monolayer, MoS₂-covered Pt (MoS₂/Pt) and bare Pt substrate were studied by way of molecular dynamics simulations. After that, a contrast study on the scratch process of MoS₂/Pt and bare Pt substrate was conducted to explore the friction reduction mechanism of the MoS₂ monolayer. As the friction reduction effect of the monolayer rests on its ability to share extra load when covering the substrate [20], the scratch process was carried out at different indentation depths.

2. Simulation Details

In our simulation models, a rigid hemisphere tip cutout from a (111)-oriented diamond crystal is placed right above the upper surface of MoS₂ monolayer, Pt(111) and MoS₂/Pt substrate at an initial height (h_0) of 10 Å, as shown in Figure 1a–c. The radius of the diamond tip was 18 Å and the size of the MoS₂ monolayer was 104.196 × 104.478 Å². Pt(111) substrate covered or not covered by a MoS₂ monolayer has the same lateral size as the monolayer. The thickness of Pt substrate is 58.902 Å. During the indentation process, the diamond tip moves vertically to the upper surface of the substrate, while during the scratch process, the diamond tip moves laterally at different indentation depths, controlled by the vertical displacement (h) of the tip. In both indentation and scratch processes, the velocity of the tip is set to 1.0 m/s. Atoms at the edge of MoS₂ are fixed in order to simulate large MoS₂ layers pinned to the substrate at the edge by Van der Waals forces. Pt atoms at the bottom are also fixed to support the substrate. For MoS₂/Pt substrate, the initial distance between the MoS₂ monolayer and the Pt(111) surface is set to 2.8 Å, the equilibrium distance where interaction energy between these two materials is the minimum. In order to learn the structure changes caused by the mechanical effect and to avoid the affection of temperature, the initial temperature is set to 0.01 K. A Langevin thermostat [23] was used in an NVE ensemble to maintain a constant temperature of 0.01 K during the simulation of indentation and scratch. The time step in this work is 0.002 ps. The number of steps is 2 million for the indentation process of the freestanding MoS₂ monolayer, 1.5 million for the indentation process of MoS₂/Pt and bare Pt substrate and 1 million for the scratch process.

A modified Stilling-Webber(SW) potential parameterized by Jin-Wu Jiang was used to describe the intra-layer interaction of MoS₂ [24]. Tersoff potential was used to describe the interaction between the carbon atoms of diamond [25]. An embedded atom method (EAM) potential was adopted to describe the interaction between Pt atoms [26]. Van der Waals forces between the diamond tip and MoS₂ monolayer were described by C-Mo and C-S Lennard-Jones(LJ) potentials. Similarly, Van der Waals forces between the diamond tip and Pt substrate were described by a C-Pt LJ potential and Pt-Mo and Pt-S LJ potentials were used to describe the Van der Waals forces between MoS₂ monolayer and Pt substrate in MoS₂/Pt system. Parameters for LJ potentials mentioned above were determined by Lorentz-Berthelot mixing rules [27], with the original ϵ and σ parameters for C-C, Pt-Pt, Mo-Mo, S-S taken from references [28–30]. Parameters for all the LJ potentials used in this work are shown in Table 1. The cutoff radius for LJ potentials was 10 Å. All the simulations were carried out with the large-scale atomic/molecular massively parallel simulator (LAMMPS) [31].

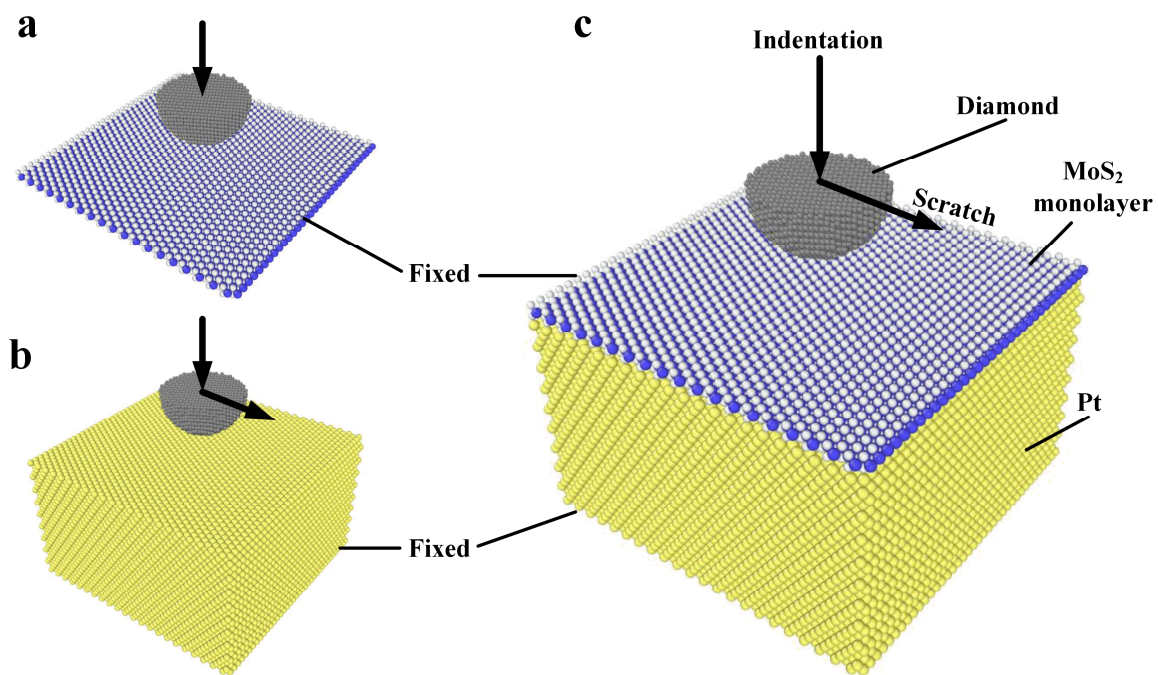


Figure 1. (a) The indentation model of freestanding MoS₂ monolayer; (b) The indentation and scratch model of Pt substrate; (c) The indentation and scratch model of MoS₂/Pt substrate.

Table 1. Parameters of Lennard-Jones (LJ) potential used in this simulation.

Pair	C-Mo	C-S	C-Pt	Pt-Mo	Pt-S
ϵ_{ij} (meV)	48.962	13.165	38.635	661.41	177.840
σ_{ij} (Å)	3.009	3.418	2.971	2.513	2.922

3. Results and Discussions

3.1. Indentation Process

Indentation of freestanding 2D layers is a common method for experimentally measuring the elasticity modulus and rupture strength of 2D materials [32]. With the MoS₂ monolayer regarded as a linear isotropic elastic material [19] and the indentation process approximated as central point loading on a clamped circular membrane [32], the relationship between indentation force and height can be deduced, as Formula (1) shows [33]:

$$F = \sigma_0^{2D} \pi(h - h_0) + E^{2D} q^3 (h - h_0)^3 / a^2, \quad (1)$$

where F is the point load at the center of the membrane, h is the vertical displacement of the tip, $h - h_0$ can represent the deflection at the center point approximately, a is the radius of MoS₂ monolayer, σ_0^{2D} and E^{2D} are the pretension and elastic modulus of the membrane, $q = 1/(1.05 - 0.15\nu - 0.16\nu^2)$ is a dimensionless constant, $\nu = 0.125$ is the Poisson ratio of bulk MoS₂ [34].

Here, in our simulation of the indentation process of freestanding MoS₂ monolayer, the elasticity properties of MoS₂ monolayer can be deduced by fitting the $F_N(h)$ curve at the elastic stage shown in Figure 2a to Formula (1). The results of E^{2D} was 199.1 N/m, which were in good agreement with the experiments [19,35]. The rupture strength was 33.8 N/m, which was very close to the results of density functional theory (DFT) calculations by Si Xiong [36].

As the freestanding MoS₂ ruptured completely in a short time during the indentation process, it was difficult to distinguish the plastic deformation stage from the force height curve before rupture,

as Figure 2a shows. However, the indentation process of MoS₂/Pt substrate showed clearly the plastic deformation stage of the MoS₂ monolayer. As shown in Figure 2b, the $F_N(h)$ curve can be divided into three stages: elastic deformation stage (see smooth part of $F_N(h)$ curve in Figure 2b, with $h < 1.07$ nm for MoS₂/Pt substrate, $h < 0.86$ nm for bare Pt substrate); plastic deformation stage (see the sawtooth shaped steps of $F_N(h)$ curve in Figure 2b, with 1.07 nm $< h < 1.99$ nm for MoS₂/Pt substrate, $h > 0.86$ nm for bare Pt substrate); and finally, the complete rupture of the MoS₂ monolayer (see the sudden drop of $F_N(h)$ curve at $h = 1.99$ nm for MoS₂/Pt substrate in Figure 2b). At the elastic and plastic deformation stages, the existence of the MoS₂ monolayer improved the load bearing capacity of the substrate, as F_N for the MoS₂/Pt substrate is always larger than the bare Pt substrate at the same indentation depth. The two force-height curves nearly overlapped after the complete rupture of the MoS₂ monolayer, which meant the anti-pressure effect of the MoS₂ monolayer completely vanished. The maximum load the MoS₂/Pt substrate can bear at the elastic deformation stage was about 62.9 nN (see Figure 2b), much smaller than 135.3 nN of the freestanding MoS₂ monolayer with a same size (see Figure 2a), which indicated different fracture criterions. In order to learn the fracture mechanism in these two cases, the structural deformations of the MoS₂ monolayer during the indentation process were studied.

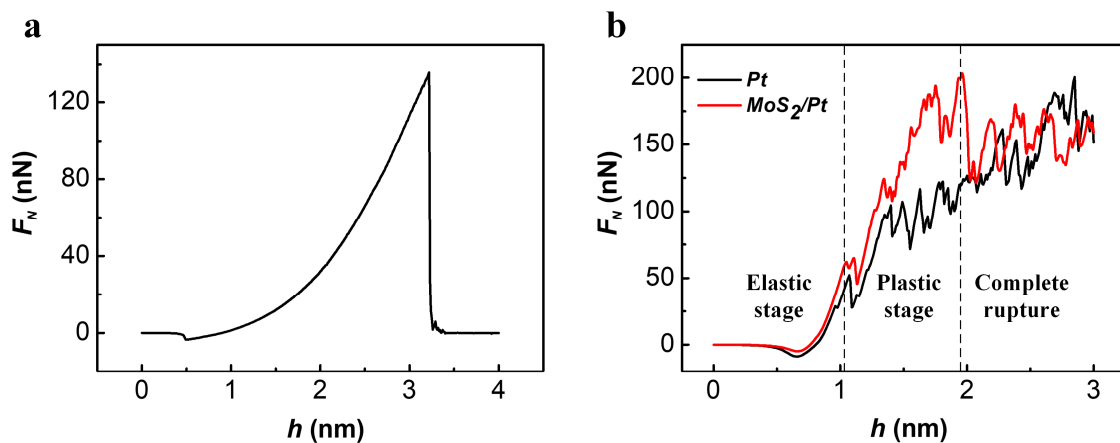


Figure 2. (a) The force-displacement curve for the indentation process of the freestanding MoS₂ monolayer; (b) The force-height curve for the indentation process of bare Pt and MoS₂/Pt substrate.

3.2. Structural Deformation

A significant structural difference between the MoS₂ monolayer and graphene is that the MoS₂ monolayer consists of a molybdenum atom layer sandwiched by two sulfur layers while graphene has only one carbon atom layer. Therefore, the deformation mechanism of the MoS₂ monolayer is different from graphene, as the out-of-plane compression of MoS₂ monolayer exists [37]. In this paper, the main structure deformations during the indentation process were divided into two types: in-plane stretch and out-of-plane compression. The distance between two adjacent Mo atoms (d_{Mo-Mo}) in the radial direction was used to represent the in-plane stretch deformation, while the distance between two opposite S atoms (d_{S-S}) in the vertical direction was used to represent the out-of-plane compression deformation [38], as shown in Figure 3a.

Compared with the freestanding MoS₂ monolayer, a higher strain rate was found in the contact region of the MoS₂/Pt substrate, as d_{S-S} and d_{Mo-Mo} changed more rapidly for atoms right under the tip in the Pt-supported MoS₂ monolayer than in the freestanding MoS₂ monolayer, as shown in Figure 3b. Furthermore, the deformation was more concentrated in the contact region for MoS₂/Pt substrate, as shown in Figure 3c,d. Similarly, with the $F_N(h)$ curve, both $d_{Mo-Mo}(h)$ and $d_{S-S}(h)$ were smooth at the elastic stage. The minimum d_{S-S} for bare MoS₂ and MoS₂/Pt substrate were very close at the end of the elasticity stage, while the maximum d_{Mo-Mo} was much smaller for MoS₂/Pt substrate than for bare MoS₂, as shown in Figure 3c,d. It can be speculated that the achievement of the strain

limit for the out-of-plane compression is the main reason for the rupture of the MoS₂ monolayer supported by Pt substrate, although both in-plane stretch and out-of-plane compression can bear load during the indentation process. The ultimate strain of out-of-plane compression was about 0.29 at the elastic stage for the indentation process of the MoS₂/Pt substrate.

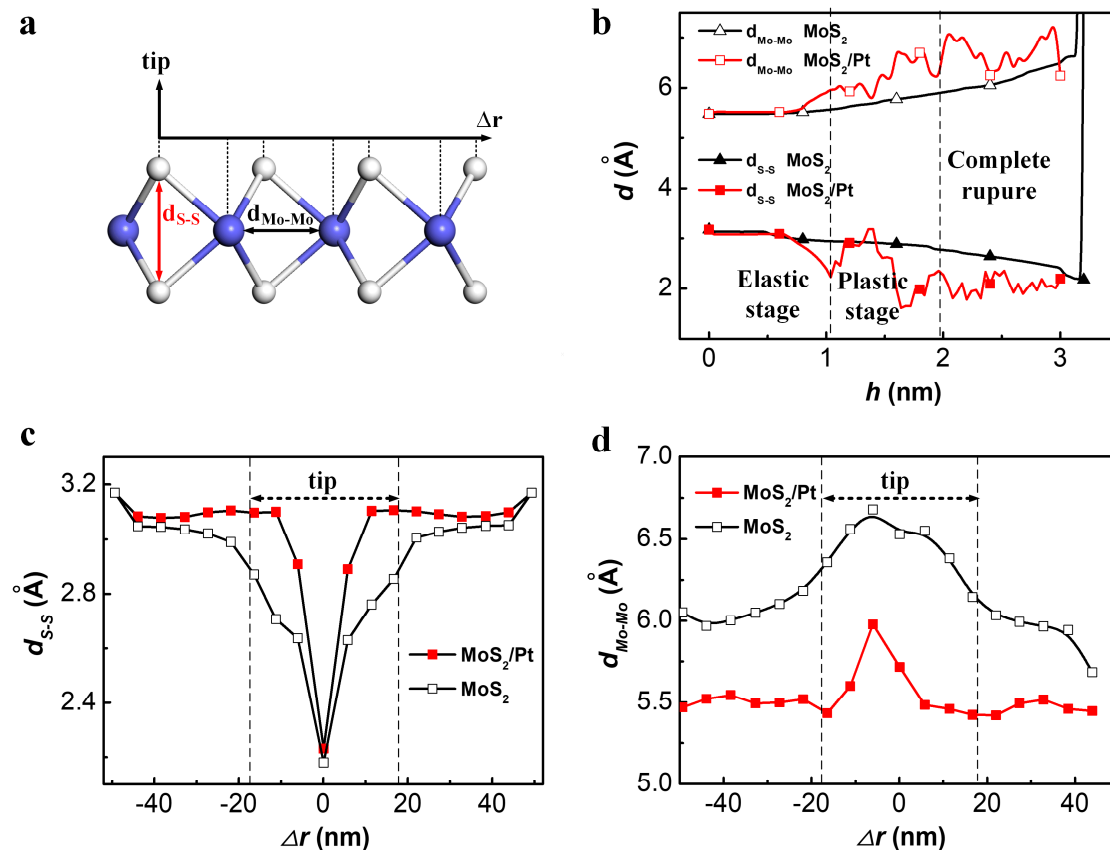


Figure 3. (a) Schematic of d_{S-S} and d_{Mo-Mo} ; (b) Evolution of d_{S-S} and d_{Mo-Mo} for atoms right under the tip during the indentation process of freestanding MoS₂ monolayer and MoS₂/Pt substrate; (c) The radial distribution of d_{S-S} for MoS₂ monolayer and MoS₂/Pt substrate at the end of elastic deformation stage; (d) The radial distribution of d_{Mo-Mo} for MoS₂ monolayer and MoS₂/Pt substrate at the end of elastic deformation stage.

3.3. Scratch Process

While the results of the indentation process showed that the anti-pressure effect of the MoS₂ monolayer is the result of structural deformation, the friction reduction effect of MoS₂ monolayer also has a strong relationship with structural deformation. In the simulation of scratch, vertical displacement of the tip varied from 0.8 nm to more than 2 nm, thus three different deformation stages of MoS₂ monolayer were covered. Figure 4 shows the friction changes with distance during the scratch process at different indentation depths. At the elastic stage, the friction force was small and the friction-distance curve was smooth, as shown in Figure 4a,b. Stick slip was found at a shallow indentation depth when $h = 0.8$ nm and disappeared when the indentation depth increased. At the plastic stage, the friction-distance curve became more and more irregular as the indentation depth increased, as shown in Figure 4c–e.

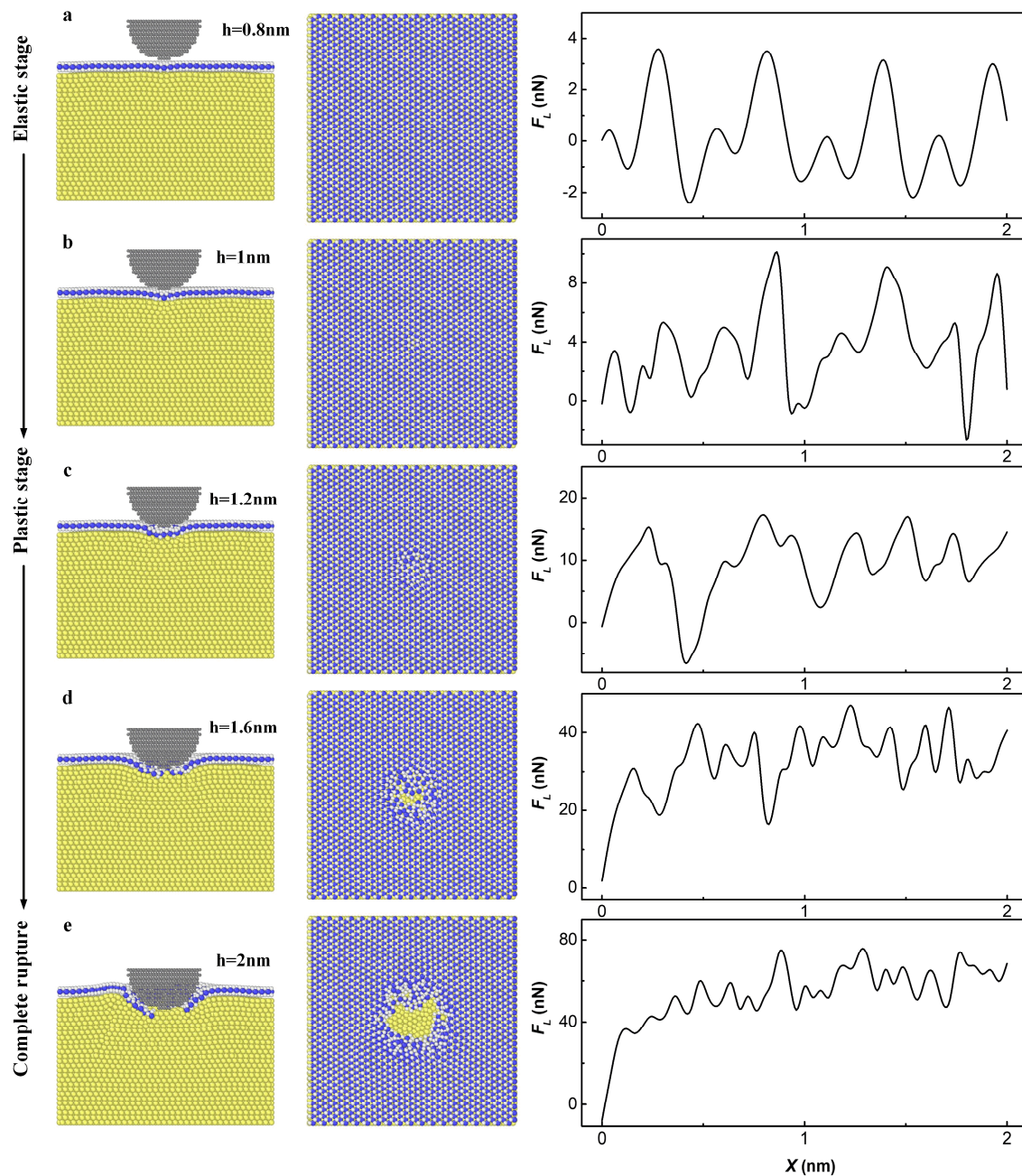


Figure 4. The left column shows the cutaway view of the simulation model, the middle column shows the top view of MoS₂/Pt substrate and the right column shows variation of friction force with sliding distance at different indentation depth: (a,b) $h = 0.8$ and 1 nm, at elastic stage of MoS₂ monolayer; (c,d) $h = 1.2$ and 1.6 nm, at plastic stage of MoS₂ monolayer; (e) $h = 2$ nm, MoS₂ monolayer completely ruptured.

The average friction force and load at different indentation depths was calculated for the scratch process of MoS₂/Pt and bare Pt substrates, as shown in Figure 5. Friction force increased with load at the elastic and plastic deformation stages. The friction reduction effect of MoS₂ monolayer relied on the degree of deformation. When MoS₂ monolayer existed, the friction coefficient was about 0.164 at the elastic stage and 0.368 at the plastic stage, which are much smaller than the 0.298 and 1.019 for the Pt substrate without MoS₂ monolayer. The turning point for the load of MoS₂/Pt substrate in Figure 5a,b stood for the complete rupture of the MoS₂ monolayer. The MoS₂ monolayer ruptured more easily

in the scratch process than in the indentation process, as the maximum load MoS₂/Pt substrate can bear before complete rupture of the MoS₂ monolayer is about 123.5 nN for $h = 1.7$ nm (see Figure 5a) during the scratch process, which is much smaller than 200.5 nN for $h = 1.99$ nm during the indentation process (see Figure 2b). After the complete rupture of the MoS₂ monolayer, both anti-pressure and the friction reduction effect vanished as F_N decreased, while F_L continued to increase with indentation depth for the MoS₂/Pt substrate.

The friction for MoS₂/Pt and bare Pt substrates were very close at the same indentation depth, while the load was much higher for MoS₂/Pt substrate, which meant MoS₂ monolayer can improve the load bearing capacity of the substrate without increasing friction. At the same load condition, the indentation depth for MoS₂/Pt substrate was smaller than for bare Pt substrate and the deformation of the substrate was also smaller, which can be a result for the lower friction coefficient of MoS₂/Pt substrate.

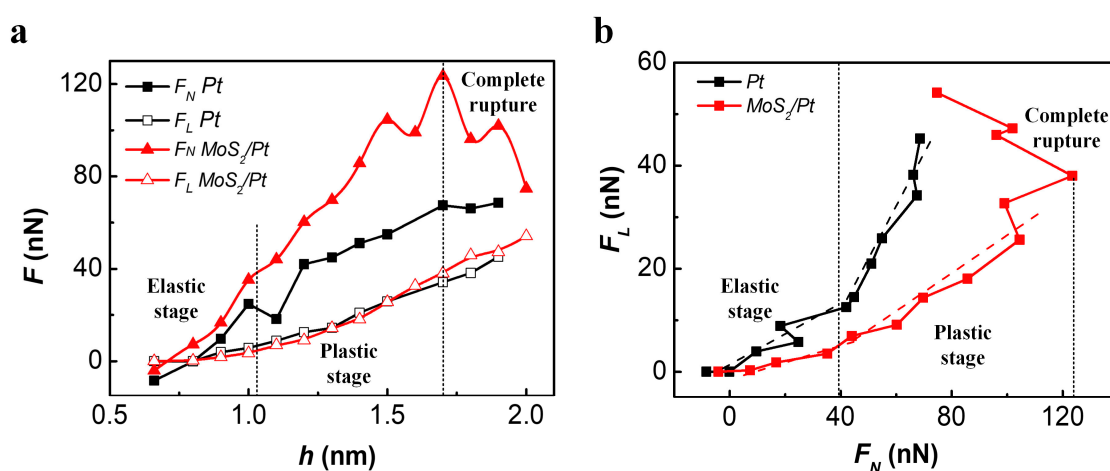


Figure 5. (a) Average load and friction varied with indentation depth during the scratch process of MoS₂/Pt and bare Pt substrates; (b) The relation between average load and friction for MoS₂/Pt and bare Pt substrates. Dashed line in (b) is a linear fitting of F_L and F_N .

4. Conclusions

In conclusion, three deformation stages of Pt-supported MoS₂ monolayer were observed: an elastic stage, a plastic stage and a completely ruptured stage. Unlike graphene, the MoS₂ monolayer can share additional load through in-plane stretch and out-of-plane compression. The rupture of MoS₂ monolayer for MoS₂/Pt system was a result of out-of-plane compression, which is very different from graphene. When covering the Pt(111) surface, MoS₂ monolayer can reduce deformation and increase the load bearing capacity of the substrate, which is a key reason for the friction reduction effect of MoS₂ monolayer. The anti-pressure and friction reduction effects of MoS₂ monolayer depend on deformation degree of the monolayer and the excellent lubrication properties will disappear after the complete rupture of the MoS₂ monolayer. These results provide a new insight into the relationship between the mechanical properties and lubrication properties of 2D materials, which can be used to predict the application prospects of different 2D materials in tribology domain.

Author Contributions: Yang Liu, Yuhong Liu and Jianbin Luo conceived and designed the project. Yang Liu performed molecular dynamics simulations and wrote the manuscript. Yuhong Liu and Tianbao Ma reviewed and revised the manuscript. All authors contributed to discussions and analyses of the results.

Funding: This research was funded by the National Natural Science Foundation of China (Grant No. 51522504) and the foundation of SKLT.

Acknowledgments: The calculations were performed on “Explorer 100” cluster system of Tsinghua University and Tianhe-II supercomputing system of the National Supercomputer Center in Guangzhou. The authors also want to acknowledge PARATERA for technical support on high-performance computation.

Conflicts of Interest: The authors declare no competing financial interest.

References

1. Gupta, A.; Sakthivel, T.; Seal, S. Recent Development in 2D Materials beyond Graphene. *Prog. Mater. Sci.* **2015**, *73*, 44–126. [[CrossRef](#)]
2. Zhu, Y.; Murali, S.; Cai, W.; Li, X.; Suk, J.W.; Potts, J.R.; Ruoff, R.S. Graphene and Graphene Oxide: Synthesis, Properties and Applications. *Adv. Mater.* **2010**, *22*, 3906–3924. [[CrossRef](#)] [[PubMed](#)]
3. Le, D.; Rawal, T.B.; Rahman, T.S. Single-Layer MoS₂ with Sulfur Vacancies: Structure and Catalytic Application. *J. Phys. Chem. C* **2014**, *118*, 5346–5351. [[CrossRef](#)]
4. Castellanos-Gomez, A. Black Phosphorus: Narrow Gap, Wide Applications. *J. Phys. Chem. Lett.* **2015**, *6*, 4280–4291. [[CrossRef](#)] [[PubMed](#)]
5. Li, C.; Xie, Z.; Chen, Z.; Cheng, N.; Wang, J.; Zhu, G. Tunable Bandgap and Optical Properties of Black Phosphorene Nanotubes. *Materials* **2018**, *11*, 304. [[CrossRef](#)] [[PubMed](#)]
6. Nemilentsau, A.; Low, T.; Hanson, G. Anisotropic 2D Materials for Tunable Hyperbolic Plasmonics. *Phys. Rev. Lett.* **2016**, *116*, 066804. [[CrossRef](#)] [[PubMed](#)]
7. Yang, N.; Yang, D.; Chen, L.; Liu, D.; Cai, M.; Fan, X. A First-Principle Theoretical Study of Mechanical and Electronic Properties in Graphene Single-Walled Carbon Nanotube Junctions. *Materials* **2017**, *10*, 1300. [[CrossRef](#)] [[PubMed](#)]
8. Lee, S.K.; Rana, K.; Ahn, J.H. Graphene Films for Flexible Organic and Energy Storage Devices. *J. Phys. Chem. Lett.* **2013**, *4*, 831–841. [[CrossRef](#)] [[PubMed](#)]
9. Soldano, C.; Mahmood, A.; Dujardin, E. Production, Properties and Potential of Graphene. *Carbon* **2010**, *48*, 2127–2150. [[CrossRef](#)]
10. Meng, F.; Han, H.; Gao, X.; Yang, C.; Zheng, Z. Experiment Study On Tribological Performances of GNPs/MoS₂ Coating. *Tribol. Int.* **2018**, *118*, 400–407. [[CrossRef](#)]
11. Luo, J.K.; Fu, Y.Q.; Le, H.R.; Williams, J.A.; Spearing, S.M.; Milne, W.I. Diamond and Diamond-Like Carbon MEMS. *J. Micromech. Microeng.* **2007**, *17*, S147. [[CrossRef](#)]
12. Bhushan, B. Nanotribology and Nanomechanics of MemS/NemS and BiomemS/BionemS Materials and Devices. *Microelectron. Eng.* **2007**, *84*, 387–412. [[CrossRef](#)]
13. Zhong, M.; Zhang, C.; Luo, J.; Lu, X. The Protective Properties of Ultra-Thin Diamond Like Carbon Films for High Density Magnetic Storage Devices. *Appl. Surf. Sci.* **2009**, *256*, 322–328. [[CrossRef](#)]
14. Wang, N.; Komvopoulos, K.; Rose, F.; Marchon, B. Structural Stability of Hydrogenated Amorphous Carbon Overcoats Used in Heat-Assisted Magnetic Recording Investigated by Rapid Thermal Annealing. *J. Appl. Phys.* **2013**, *113*, 083517. [[CrossRef](#)]
15. Kim, K.; Lee, H.; Lee, C.; Lee, S.; Jang, H.; Ahn, J.; Kim, J.; Lee, H. Chemical Vapor Deposition-Grown Graphene: The Thinnest Solid Lubricant. *ACS Nano* **2011**, *5*, 5107–5114. [[CrossRef](#)] [[PubMed](#)]
16. Berman, D.; Erdemir, A.; Sumant, A.V. Few Layer Graphene to Reduce Wear and Friction on Sliding Steel Surfaces. *Carbon* **2013**, *54*, 454–459. [[CrossRef](#)]
17. Xie, H.; Jiang, B.; Dai, J.; Peng, C.; Li, C.; Li, Q.; Pan, F. Tribological Behaviors of Graphene and Graphene Oxide as Water-Based Lubricant Additives for Magnesium Alloy/Steel Contacts. *Materials* **2018**, *11*, 206. [[CrossRef](#)] [[PubMed](#)]
18. Berman, D.; Erdemir, A.; Sumant, A.V. Graphene: A New Emerging Lubricant. *Mater. Today* **2014**, *17*, 31–42. [[CrossRef](#)]
19. Bertolazzi, S.; Brivio, J.; Kis, A. Stretching and Breaking of Ultrathin MoS₂. *ACS Nano* **2011**, *5*, 9703–9709. [[CrossRef](#)] [[PubMed](#)]
20. Klemenz, A.; Pastewka, L.; Balakrishna, S.G.; Caron, A.; Bennewitz, R.; Moseler, M. Atomic Scale Mechanisms of Friction Reduction and Wear Protection by Graphene. *Nano Lett.* **2014**, *14*, 7145–7152. [[CrossRef](#)] [[PubMed](#)]
21. Zhao, J.; He, Y.; Wang, Y.; Wang, W.; Yan, L.; Luo, J. An Investigation on the Tribological Properties of Multilayer Graphene and MoS₂ Nanosheets as Additives Used in Hydraulic Applications. *Tribol. Int.* **2016**, *97*, 14–20. [[CrossRef](#)]

22. Chen, Z.; Liu, X.; Liu, Y.; Gonsel, S.; Luo, J. Ultrathin MoS₂ Nanosheets with Superior Extreme Pressure Property as Boundary Lubricants. *Sci. Rep.* **2015**, *5*, 12869. [[CrossRef](#)] [[PubMed](#)]
23. Dong, Y.; Li, Q.; Martini, A. Molecular Dynamics Simulation of Atomic Friction: A Review and Guide. *J. Vac. Sci. Technol. A* **2013**, *31*, 30801. [[CrossRef](#)]
24. Jiang, J.; Park, H.S.; Rabczuk, T. Molecular Dynamics Simulations of Single-Layer Molybdenum Disulphide (MoS₂): Stillinger-Weber Parametrization, Mechanical Properties and Thermal Conductivity. *J. Appl. Phys.* **2013**, *114*, 064307. [[CrossRef](#)]
25. Tersoff, J. Chemical Order in Amorphous Silicon Carbide. *Phys. Rev. B* **1994**, *49*, 16349–16352. [[CrossRef](#)]
26. Zhou, X.W.; Johnson, R.A.; Wadley, H. Misfit-Energy-Increasing Dislocations in Vapor-Deposited CoFe/NiFe Multilayers. *Phys. Rev. B* **2004**, *69*, 144113. [[CrossRef](#)]
27. Li, L.; Xia, Z.H.; Curtin, W.A.; Yang, Y.Q. Molecular Dynamics Simulations of Interfacial Sliding in Carbon-Nanotube/Diamond Nanocomposites. *J. Am. Ceram. Soc.* **2009**, *92*, 2331–2336. [[CrossRef](#)]
28. Girifalco, L.A.; Hodak, M.; Lee, R.S. Carbon Nanotubes, Buckyballs, Ropes and a Universal Graphitic Potential. *Phys. Rev. B* **2000**, *62*, 13104. [[CrossRef](#)]
29. Toghraie, D.; Mokhtari, M.; Afrand, M. Molecular Dynamic Simulation of Copper and Platinum Nanoparticles Poiseuille Flow in a Nanochannels. *Phys. E* **2016**, *84*, 152–161. [[CrossRef](#)]
30. Varshney, V.; Patnaik, S.S.; Muratore, C.; Roy, A.K.; Voevodin, A.A.; Farmer, B.L. MD Simulations of Molybdenum Disulphide (MoS₂): Force-Field Parameterization and Thermal Transport Behavior. *Comput. Mater. Sci.* **2010**, *48*, 101–108. [[CrossRef](#)]
31. Plimpton, S. Fast Parallel Algorithms for Short-Range Molecular Dynamics. *J. Comput. Phys.* **1995**, *117*, 1–19. [[CrossRef](#)]
32. Lee, C.; Wei, X.; Kysar, J.W.; Hone, J. Measurement of the Elastic Properties and Intrinsic Strength of Monolayer Graphene. *Science* **2008**, *321*, 385–388. [[CrossRef](#)] [[PubMed](#)]
33. Komaragiri, U.; Begley, M.R.; Simmonds, J.G. The Mechanical Response of Freestanding Circular Elastic Films Under Point and Pressure Loads. *J. Appl. Mech.* **2005**, *72*, 203–212. [[CrossRef](#)]
34. Lovell, M.R.; Khonsari, M.M.; Marangoni, R.D. A Finite Element Analysis of the Frictional Forces Between a Cylindrical Bearing Element and MoS₂ Coated and Uncoated Surfaces. *Wear* **1996**, *194*, 60–70. [[CrossRef](#)]
35. Castellanos Gomez, A.; Poot, M.; Steele, G.A.; van der Zant, H.S.; Agraït, N.; Rubio Bollinger, G. Elastic Properties of Freely Suspended MoS₂ Nanosheets. *Adv. Mater.* **2012**, *24*, 772–775. [[CrossRef](#)] [[PubMed](#)]
36. Xiong, S.; Cao, G. Molecular Dynamics Simulations of Mechanical Properties of Monolayer MoS₂. *Nanotechnology* **2015**, *26*, 185705. [[CrossRef](#)] [[PubMed](#)]
37. Peña-Álvarez, M.; del Corro, E.; Morales-García, Á.; Kavan, L.; Kalbac, M.; Frank, O. Single Layer Molybdenum Disulfide Under Direct Out-of-Plane Compression: Low-Stress Band-Gap Engineering. *Nano Lett.* **2015**, *15*, 3139–3146. [[CrossRef](#)] [[PubMed](#)]
38. Lorenz, T.; Joswig, J.; Seifert, G. Stretching and Breaking of Monolayer MoS₂—An Atomistic Simulation. *2D Mater.* **2014**, *1*, 011007. [[CrossRef](#)]

